Towards Gravitational Wave Templates for Hierarchical Triple Systems: A Preliminary Study

MSc Dissertation

Submitted to the Department of Physics and Electronics

Submitted by

Mukhil Chandrakumar - 2347336

in partial fulfillment of requirements for

Master of Science in Physics
2025

under the supervision of

Dr. Arun Kenath

Associate Professor
Department of Physics and Electronics

Declaration

Date: 04/02/2025

I, **Mukhil C**, hereby declare that this thesis/ dissertation titled ***"Towards Gravitational Wave Templates for Hierarchical Triple Systems: A Preliminary Study"***, submitted to CHRIST (Deemed to be University), Bangalore, toward the partial fulfillment of the requirements for the degree of **Master of Science in Physics**, is an original work carried out by me under the **supervision of Dr. Arun Kenath** and has not formed the basis for the award of any degree or diploma, in this or any other institution or university. I have sincerely tried to uphold academic ethics and honesty in the project process. Whenever a piece of external information or statement or result is used, then that has been duly acknowledged and cited.

Mukhil C
Reg.No.: 2347336

Certification

Date: 04/02/2025

This is to certify that the thesis/dissertation titled ***"Towards Gravitational Wave Templates for Hierarchical Triple Systems: A Preliminary Study"*** submitted by **Mukhil C**, in partial fulfillment of the requirements for the degree of **M.Sc. Physics** in **Department of Physics and Electronics**, is an original work carried out by him under my supervision.

Dr. Arun Kenath
Associate Professor
Department of Physics and Electronics
CHRIST (Deemed to be University)

Acknowledgement

I express my gratitude to all those who have supported me throughout my journey toward the completion of this Master's Dissertation. This work would not have been possible without the guidance, patience, and encouragement of many individuals.

First and foremost, I am deeply grateful to my supervisor, Dr. Arun Kenath, for his invaluable guidance and continuous support throughout this research. His insightful feedback and patience have played a crucial role in shaping this study, helping me navigate challenges, and refining my ideas. Dr. Kenath's willingness to provide constructive criticism while allowing me the freedom to explore my own approach has been instrumental in my academic growth.

Additionally, I would like to express my sincere appreciation to my friends and colleagues for their stimulating discussions and unwavering encouragement. They have been the most open-minded individuals I have ever met, always willing to discuss their own projects without hesitation. These discussions have provided insights I would not have gained otherwise and have greatly enriched my research. Their companionship has made this challenging journey much more manageable.

Finally, I extend my deepest gratitude to my family for their unconditional support and patience throughout this journey. Without their encouragement, I could not have completed this project, and for that, I am forever grateful.

This thesis is dedicated to all those who have, directly or indirectly, contributed to its completion.

Abstract

The recent advancements in gravitational wave (GW) astronomy have allowed for many insights into the workings of the universe and also were useful for testing the Theory of General Relativity. This study aims to do a preliminary analysis of gravitational wave (GW) emission from hierarchical triple systems in toward the creation of a Python pipeline for generating GW templates for matched filtering signals from such systems. Gravitational waves are significantly impacted by the complex dynamics of triple systems, particularly through Kozai-Lidov (KL) oscillations. These oscillations, induced by the interaction between an inner binary and a distant third body, can lead to high eccentricity states that enhance GW emission. The work fills a notable gap by assessing GW signal detectability in present and future detectors and provide a base insight into the evolutionary dynamics of GWs in triple systems, highlighting their relevance for upcoming observational missions.

Contents

1 Introduction 1
2 Gravitational Waves 3
2.1 Mathematics behind GW production 3
2.2 GW classification 6
2.3 GW frequency ranges 7
3 Kozai-Lidov mechanism 8
4 Lense-Thirring effect 10
5 Research Gap 11
5.1 Research Statement 11
5.2 Objectives 11
5.3 Methodology 12
6 Results 12
6.1 Parameter Determination 12
6.2 GWs from highly eccentric orbits 15
6.3 Detector Noise Curves 16
6.4 Frequency Ringdown 19
7 Future Work 20
7.1 Orbit Evolution 20
7.2 GW Modelling 20
References 22

1 Introduction

The existence of gravitational waves (GW) was first proved theoretically by Einstein using his theory of General Relativity (GR) in the year 1916. He predicted that GWs behaved in a way similar to that of electromagnetic radiation, but they are produced by quadrupole sources and not dipoles. This allowed him to describe the rate of energy decay due to GW emission. The first proof for GWs, though indirect, came when the first binary neutron star system discovered by Russell Hulse and Joseph Taylor in 1974, aptly named the Hulse–Taylor pulsar, exhibited a regularly varied pulsating rate, indicating a gradually shrinking orbit and hence proving the GR prediction of energy decay. The first direct detection of a GW, however, would not occur until 2015 when the Laser Interferometer Gravitational-Wave Observatory (LIGO) detected the GW from a binary black hole (BBH) GW150914, which has paved the way for many new research efforts in the field. [1]

The GW signal is causal effect of a perturbation of the spacetime metric. This perturbation could be caused by any asymmetry on spacetime such as a binary system, non-uniformities on compact objects such as Neutron Stars (NSs), density fluctuations in the inflationary period, etc. The GW signal is classified into three phases: the inspiral, the merger and the ringdown phases. The inspiral phase is characterized by the slow orbital decay of a compact binary due to gravitational wave emission, leading to an increase in frequency and amplitude. The merger phase occurs when the two objects coalesce, producing the peak gravitational wave signal as they dynamically interact. The ringdown phase is dominated by the relaxation of the newly formed remnant, emitting quasi-normal gravitational wave modes that decay over time [2]. GW signals can originate from a variety of sources, astrophysical and stochastical, including isolated binary mergers, dynamical interactions in dense star clusters, inflationary era fluctuations, cosmic strings, etc.

The LIGO detectors (in Livingston and Hanford) are, in simple terms, Michelson Interferometers, with two arms, of length 4km, kept perpendicular to each other, forming an L shaped interferometer. These detectors operate in observing runs interspersed with commissioning runs for repair and upgrades. The advanced LIGO (aLIGO) detectors have had 3 completed runs (O1, O2, O3) with O4 currently ongoing. These detectors have been joined by the European Virgo Interferometer, in O2 [3], and Kamioka Gravitational Wave Detector (KAGRA), in O3, forming the LIGO-Virgo-KAGRA (LVK) collaboration[4]. They currently have a working frequency range from 10Hz to 10kHz.

This network of detectors have contributed greatly to the detection of GW events, mainly mergers of compact objects, with over 100+ detections over the decade of their operation.

But as seen by the frequency sensitivity of the ground-based detectors, caused by mulitiple sources of noise in the detector, they will not be able to detect signals at frequencies lower than 10Hz. To detect signals at lower frequencies, the arms of the detector must be made larger. While it is possible to extend the arm length or ground based detector, as seen in the proposed 40km Cosmic Explorer, it is much easier to have a space based detector whose arm length could be kept at millions of kilometers. Hence, the existence of the in-development Laser Interferometer Space Antenna (LISA), a collaboration between National Aeronautics and Space Administration (NASA) and European Space Agency (ESA), to be launched in the 2030s. It consists of three satellites, which consists of interferometer test masses and 'the laser cavities, kept at the corners of a triangular arrangement whose arm length (i.e. side length of the triangle) is around 2.5 million kilometers. This satellite constellation will be put on the Earth-Sun Orbit. As previously said, the arm length of LISA will allow for detected signals at much lower frequencies, with a frequency sensitivity range of 10μHz to 1Hz. This allows for the detection of signal from Supermassive Black Hole (SMBH) mergers, etc. The detector will also detect the Stochastic Gravitational Wave Background (SGWB), whose signals appear at lower frequencies. [5]

These sensitivities allow for the detection of eccentric binaries whereas only binaries with circular orbits are detected in LVK. Eccentric binaries are highly efficient GW emitters and hence appear at lower frequencies compared to circular orbits. These kinds of eccentric systems must dominate the detections compared to circular orbit system but due to the circularization of the eccentric orbit by GW emission, by the time of merger, the orbit has almost completely circularized, causing it to appear in the LVK band as a binary in a circular orbit. Some residual eccentricity may remain, but has a very neglible effect on the signal.

The formation of such eccentric orbits can be attributed to dynamical interaction with multiple bodies. One such cause for eccentricity is by the Kozai-Lidov mechanism appearing in hierarchical triple systems. A triple system is considered to be a hierarchical triple system (HTS) if there are two masses acting as an inner binary and the third larger mass, at a great distance away from the inner binary, forms an outer binary with the center of mass of the inner binary. Here, the third mass acts as a perturber on the inner

binary. By the KL mechanism, there occurs a secular evolution of eccentricity of the inner binary and it's inclination with respect to the outer binary plane. This effect occurs when the inner binary plane is inclined at an angle between 40° and 140° with respect to the outer binary plane. This allows eccentricity to increase at the cost of inclination. [6]

This study focuses on developing a more accurate model for gravitational wave (GW) emission from hierarchical triple systems by conducting a preliminary study on the detectability of such systems in our present and future detectors and providing a theoretical framework for the evolution of the system and modeling the GWs. Section 2 focuses on how GR allows for GW emission, the classification of sources, and signals. It also provides the mathematical explanation for the GW emission from eccentric binaries. Section 3 provides an introduction to the Kozai Lidov mechanism and it's applications in GW research. Section 4 provides a brief note on the Lense-Thirring effect, which appear in the presence of a third spinning SMBH in the HTS. This effect is constrained in our parameter space in the current project but will be included in our future work. Section 5 explains the research gap and the methodology of our work. We finally present our current results in Section 6 with future work mentioned in Section 7.

2 Gravitational Waves

2.1 Mathematics behind GW production

The basic postulate of GR is that any mass bends spacetime and results in spacetime curvature. We begin our understanding of this postulate from the metric, which gives us the curved spacetime distance between two events [7, 8], defined by

$$ds^2 = g_{ik}dx^i dx^k \tag{2.1.1}$$

where g_{ik} defines the curvature of spacetime. This curvature is quantified by the Riemmannian Tensor [7, 8], which is a function of the first and second derivative of the metric tensor given by

$$R_{iklm} = \frac{1}{2}[g_{kl,im} + g_{im,kl} - g_{km,il} - g_{il,km}] \tag{2.1.2}$$

Thus, if the Riemmann tensor vanishes everywhere, spacetime is flat. By process of contraction, we can find the Ricci tensor [7, 8], which is a representation of the degree of difference between a given metric tensor locally and an Euclidean space, given by

$$R_{km} = g^{il}R_{iklm} = \frac{1}{2}[g^i_{k,im} + g^i_{m,kl} - g^{il}g_{km,il} - g^l_{l,km}] \tag{2.1.3}$$

Contracting the equation further we get the Ricci scalar or scalar curvature [7, 8],

$$R = g^{ik}R_{ik} = R^k_k \tag{2.1.4}$$

Using these equations, we finally arrive at Einstein's field equations[7, 8],

$$G_{ik} = R_{ik} - \frac{1}{2}g_{ik}R = \frac{8\pi G}{c^4}T_{ik} \tag{2.1.5}$$

where G_{ik} is the Einstein tensor, T_{ik} is the stress energy tensor, G is the gravitational constant and c is the speed of light. Any change in the stress energy tensor indicates a matter distribution change which in turn gives rise to a modified gravitational field. Thus metric is perturbed and the change in the metric tensor [7, 8] is given by

$$g_{ik} = \eta_{ik} + h_{ik} \tag{2.1.6}$$

where h_{ik} is the perturbation induce in the spacetime metric and can be considered to be a sign of the GW.

However, finding the tensor using the Einstein field equations is difficult and hence we shall consider the weak field approximation along with the linearized theory of gravity, where gravitational fields are weak in the sense that for given $g_{ik} = \eta_{ik} + h_{ik}$, $|h_{ik}| << 1$ i.e. the perturbation is very small and only considers terms linear in h_{ik}. This approximation gives the proper result for the generation and propagation of GW [7, 8]. Thus, we have

$$R_{iklm} \cong \frac{1}{2}[h_{im,kl} + h_{kl,im} - h_{km,il} - h_{il,km}] \tag{2.1.7}$$

But as these conditions do not uniquely specify any coordinate system, we are free to apply any coordinate transformation without violating these conditions. So, we can apply another auxilliary condition [7] to this situation

$$\Psi^k_i = h^k_i + \frac{1}{2}h\delta^i_k \tag{2.1.8}$$

such that

$$\Psi^k_{i,k} = [h^k_i + \frac{1}{2}h\delta^i_k]_{,k} = \frac{\partial}{\partial x^k}[h^k_i + \frac{1}{2}h\delta^i_k] = 0 \tag{2.1.9}$$

where Ψ^k_i are gravitational potentials and the above conditions are called gauge equations. The transformation that satisfies (2.1.9) is found [7] to be

$$x^{'i} = x^i + \xi^i, \quad \Box\xi^i = 0 \tag{2.1.10}$$

where ξ^i are infinitesimal quantities and thus result in an infinitesimal coordinate transformation. Also, the symbol $\Box$ represents the D'Alembertian operator [7] given by

$$\Box = \eta^{ik}\frac{\partial^2}{\partial x^i \partial x^k} = \frac{\partial^2}{\partial t^2} - \nabla^2 \tag{2.1.11}$$

Now as (2.1.9) holds, we can find the required tensors in our weak field approximations [7],

$$R_{ik} \cong \frac{1}{2}\Box h_{ik} \quad and \quad R \cong \frac{1}{2}\Box h$$
$$R_{ik} + \frac{1}{2}\eta_{ik}R \cong \frac{1}{2}\Box \Psi_{ik} \tag{2.1.12}$$

Comparing the above equation to Einstein's field equations (see 2.1.5), we get

$$\Box \Psi_{ik} = \frac{16\pi G}{c^4}T_{ik} \tag{2.1.13}$$

which is a general wave equation for a given source. Let us consider a plane wave solution for the equation and assume that apart from the wave, the space is empty (i.e.$T_{ik} = 0$). Then the wave equation in (2.1.13) results in

$$\Box \Psi_{ik} = 0 \tag{2.1.14}$$

which is a 3D wave equation constrained by the Hilbert gauge condition, $\delta_i \Psi_{ik} = 0$. For the gauge transformation, we require a coordinate tranformation given by (2.1.10) where η^i satisfies the condition, $\delta_i \delta^i \eta^i = 0$. Note that if this condition is not satisfied, new gravitational field does not agree with the Hilbert gauge condition and hence cannot exist. The simplest solution for the gravitational wave equation [7] is

$$\Psi_{ik} = A^{ik} e^{iK_\alpha x^\alpha} \tag{2.1.15}$$

where A^{ik} represents the amplitude and polarization of the wave and K_α gives the propagation direction and frequency of the wave where the Hilbert gauge condition, in this case, requires $A^{ik}k_\alpha = 0$. This condition also implies orthogonality of the two quantities but we shall focus only on the real part of the solution. Take a coordinate system $x^0 = ct$, $x^1 = x$, $x^2 = y$, $x^3 = z$. As space is empty, from (2.1.14), we get

$$\Box h_{ik} = 0 \tag{2.1.16}$$

If the plane wave is travelling along the x direction, all of h_{ik} are functions of $(t - x)$. Thus, our gauge conditions become

$$0 = \frac{\partial \Psi_i^1}{\partial x} + \frac{\partial \Psi_i^0}{\partial t} = -\frac{\partial \Psi_i^1}{\partial t} + \frac{\partial \Psi_i^0}{\partial t} \tag{2.1.17}$$

such that $[\Psi_i^0 - \Psi_i^1]$ is a function of x only. But as we are allowing only wave type functions, we can set this to zero and we get $\Psi_i^0 = \Psi_i^1$ Now, from (2.1.10), we use ξ^i as a explicit function of x to make the terms in Ψ_{ik} vanish. However, we see that we cannot render Ψ_2^3 and $\Psi_2^2 + \Psi_3^3$ quantities to zero. So. in terms of h_{ik}, the plane wave is characterized by 2 functions,

$$h_{22} = -h_{33} \quad \text{and} \quad h_{23} \tag{2.1.18}$$

To find the power loss of a system due to GW emission, we assume that we have a compact time dependent source confined to a 3-volume V so that the GW emerging from source appears as a plane wave passing by to an observer. Using local coordinates with the x-axis being the direction of propagation of wave, from (2.1.18), for a source at distance R_o, we have

$$h_{23} = \frac{2G}{3R_o}\dddot{D}_{23} \quad \text{and} \quad h_{22} - h_{33} = \frac{2G}{3R_o}(\dddot{D}_{22} - \dddot{D}_{33}) \tag{2.1.19}$$

where $D_{\alpha\beta}$ is the quadrupole moment tensor of source defined by

$$D_{\alpha\beta} = \int \rho(3x^\alpha x^\beta - \delta_{\alpha\beta}r^2)dV \tag{2.1.20}$$

where coordinates x^α are Cartesian and r is Euclidean distance from origin of a point with these coordinates. From an analogous comparison to that of electromagnetic radiation from oscillating dipole, we find the power radiation by the GW source to be

$$P = \frac{G}{45c^5}\dddot{D}^2_{\alpha\beta} \tag{2.1.21}$$

2.2 GW classification

We can classify GWs based on their source/origin [9]. They can be broadly divided into four types:

1. **Continuous GWs**: These GWs are thought to be produced by a single massive object, like a neutron star. These signals can be attributed to physical asymmetries in the object. These GWs are very weak (order of 10^-25 or lower). In general, the characteristic amplitude of GW from a neutron star can be given by the equation

$$h = \frac{If_o^2\epsilon}{r} \tag{2.2.1}$$

where f_o is the frequency of emitted signal, I is the moment of inertia of the neutron star, ϵ is the ellipticity which describes the asymmetric nature of the neutron star and r is the distance of neutron star from detector.

2. **Inspiral GWs**:Binary objects such as binary black holes (BBH) and binary neutron stars (BNS), are one of the most prominent source of GW. The constituent objects of the binary system generate GW while spiralling towards each other for long periods of time until merger. There also exist triple systems of such objects which also produce GWs on a similar basis.

3. **Stochastic GWs**:Compared to the above two sources of GWs, which are of higher intensity, there exists weaker GW signals that seem to come from all over the cosmos, similar to the cosmic microwave background (CMB) radiation, thus being given an analogous name, Gravitational Wave Background (GWB) and referred to as stochastic GW signal due to their random waveform.

4. **GW Transient/Burst GWs**:If a star collapses in a non spherical manner, then a GW signal may be produced for a very small time period (in the order of few milliseconds). However, as modelling collapse dynamics is a difficult challenge, these signal are difficult to detect. One ways of detection is by analysing for excess power in the interferometric data. As the strains of these signals are of the order $10^{-}7$ and occur for a short burst, these signal can only be detected by the LIGO/VIRGO, if they take place in this galaxy. But, detection probability of such signal is very low as rate of supernovae formation is very low.

2.3 GW frequency ranges

The frequency classification of GW [7] is:

1. **Ultra High Frequency (UHF) band**: **Frequencies above 1THz**. Detection by optical and terahertz resonators.

2. **Very High Frequency (VHF) band**: **Frequency range of 100kHz - 1THz**. Detection by optical interferometers, gaussian beam detectors, microwave resonators or wave-guide detectors.

3. **High Frequency (HF) band**: **Frequency range of 10Hz - 100kHz**. Detection by ground laser interferometric ground observatories such as LIGO, VIRGO, KAGRA. Low temperature resonators are also used.

4. **Middle Frequency (MF) band**: **Frequency range of 0.1Hz - 10Hz**. Detection by space interferometric detectors, They have short arm length (100km -10000km)

5. **Low Frequency (LF) band**: **Frequency range of 100nHz - 0.1Hz**. Detection done primarily by sace based laser interferometers.

6. **Very Low Frequency (VLF) band**: **Frequency range of 300pHz - 100nHz**. Detection by Pulsar Timing Arrays (PTAs).

7. **Ultra Low Frequency (ULF) band**: **Frequency range of 10fHz - 300pHz**. Detection requires investigation of quasar positions and proper motions

8. **Extremely Low (Hubble) Frequency (ELF/HF) band**: **Frequency range of 1aHz - 10fHz**. Detection by CMB experiments.

9. **Beyond Hubble Frequency (BHF) band**: **Frequencies below 1aHz**. Direct verification is nearly impossible. Indirect evidence can be found by inflationary models

3 Kozai-Lidov mechanism

The Kozai-Lidov (KL) mechanism [10, 11] is a dynamical phenomenon observable in such hierarchical triple systems, wherein a tertiary body affects the orbital motion of a smaller object encircling a larger mass. This effect was concurrently identified in the 1960s by the endeavors of Yoshihide Kozai of Japan and Mikhail Lidov of Russia. It describes a periodic modulation of the argument of pericenter within an orbit, consequentially inducing an interchange between the orbit's eccentricity and inclination over durations that exceed the orbital periods by a significant margin, i.e., due to the interplay between the inner and outer binaries, leading to periodic fluctuations in the eccentricity of the inner binary and the angular displacement between the two binaries.

Analytically, the Hamiltonian for a hierarchical tri-body system can be decomposed into two distinct segments pertaining to the independent evolution of the inner and outer binaries, augmented by a third segment that encapsulates the interaction between their orbits [12]. This is given as:

$$\mathcal{H}_{total} = \mathcal{H}_{inner} + \mathcal{H}_{outer} + \mathcal{H}_{perturbation} \tag{3.1}$$

In the context of hierarchical astrophysical systems, the coupling term therein is systematically developed as a power series in the parameter α, which represents the ratio of the semi-major axes of the inner to the outer orbiting bodies, and is characteristically minuscule in such expansive systems. Owing to the swift convergence of this perturbative

series, the primary behavioral dynamics of a hierarchical triple system are discernibly influenced by the principal constituents of the series expansion, colloquially designated as the quadrupole (Q), octupole (O), and hexadecapole (H) order terms [12]. These terms tell us the conditions/constraints put on the system to help simplify and determine the dynamics of the system.

In the realm of gravitational wave astrophysics, the KL mechanism is posited to hold considerable significance. Simulations suggest that a significant fraction of binary systems, influenced by third-body perturbations, maintain an eccentricity exceeding 0.1 upon entering the detection range of instruments like LIGO. Furthermore, induced by KL oscillations, increased eccentricities are anticipated to abbreviate the merger times of these systems. Hence, computing the incidence of colliding eccentric binaries, particularly within densely populated celestial fields, necessitates a precise integration of third-body dynamics alongside the post-Newtonian relativistic corrections [12].

A fundamental assumption underlying this configuration is that the gravitational influence exerted by the tertiary companion on the inner binary's orbit is minimal when compared to the interaction forces between the two inner bodies. In the context of a simpler two-body Newtonian framework, a bound system follows an elliptical orbit that is characterized by six orbital elements: semi-major axis a, eccentricity e, inclination i, argument of periastron ω, longitude of ascending node Ω, and mean anomaly M. However, in the hierarchical three-body case, perturbations caused by the tertiary companion impact the motion within the inner binary, resulting in a deviation from the isolated binary's expected elliptical trajectory [6].

To account for these perturbations, the concept of an osculating orbit [13] is introduced, providing an approximate trajectory that can be described by an elliptical path defined by the aforementioned six orbital elements, derived from the system's instantaneous position and velocity at any given moment. As for the outer orbit, this is considered as the motion of the inner binary's center of mass as it rotates around the tertiary companion, which can also be represented as another osculating orbit. In this framework, the masses of the inner binary components are denoted m_1 and m_2, while the tertiary companion has a mass m_3. To distinguish between the inner and outer orbits, subscripts "in" and "out" are used respectively. In such systems, the orbital periods of the inner and outer

binary is given by

$$P_{in} = 2\pi\sqrt{\frac{a_{in}^3}{Gm_{in}}} \quad , \quad P_{out} = 2\pi\sqrt{\frac{a_{out}^3}{Gm_{out}}} \tag{3.2}$$

At a particular relative inclination I, a secular change of orbital elements may occur where under certain conditions, an oscillation between the values of the eccentricity and relative inclination occurs with the relative equation defined as the argument between the inner and outer orbital planes [10, 11] and is given by

$$cosI = cos\, i_{in}\, cos\, i_{out} + sin\, i_{in}\, sin\, i_{out}\, cos(\Omega_{in} - \Omega_{out}) \tag{3.3}$$

which results in the secular exchange of e_{in} and I with the conserved value [14] of

$$\Theta = (1 - e_{in}^2)\, cos^2 I \tag{3.4}$$

with the condition for KL oscillation, provided $m_1 << m_2, m_3$ and the outer orbit is circular is

$$0 \leq |cosI| \leq \sqrt{\frac{3}{5}} \tag{3.5}$$

Do note that the KL oscillation will occur even if m_1 is not much smaller than m_2, m_3.

The KL oscillation timescale [15] is given by

$$t_{\rm KL} \sim P_{\rm in}\frac{m_{\rm in}}{m_3}\left(\frac{a_{\rm out}}{a_{\rm in}}\right)^3 \left(1 - e_{\rm out}^2\right)^{\frac{3}{2}} \tag{3.6}$$

4 Lense-Thirring effect

The Lense-Thirring (LT) effect is a general relativistic correction to the precession of a gyroscope in the presence of a large rotating mass. This causes the relative orbital nodes of the gyroscope to precess[16].

Recent studies have shown changes in KL oscillations caused due to GR effects involving a SMBH. If the third body is a rapidly rotating SMBH, then LT effect might become important in changing the evolution of eccentricity excitation from the usual KL oscillation. The effect appears in the 1.5PN order [17, 18, 19].

For a rotating black hole, the spin angular momentum[6, 17, 19] is given as $S_3 = \chi_3 G m_3^2/c$, where χ_3 is the spin parameter, and the outer orbital angular momentum [17, 19] is given as

$$L_{out} \;=\; \mu_{out}[G(1 - e_{out}^2)a_{out}M] \tag{4.1}$$

where M is the total mass of the gyroscope and the reduced mass of the outer orbit is defined by

$$\mu_{out} = \frac{m_{in}m_3}{m_{out}} \tag{4.2}$$

The timescale of the orbit-averaged precession of L_{out} around S_3 [17, 19] is given by

$$t_{L_{\rm out}S_3} = \frac{2c^2(1-e_{\rm out}^2)^{\frac{3}{2}}a_{\rm out}^3}{GS_3\,(4+3m_{\rm in}/m_3)} \tag{4.3}$$

5 Research Gap

When a triple system is formed with a stellar mass black hole binary (BHB) forming an inner orbit and an SMBH being the perturber and forms the outer orbit, by the KL mechanism, we can get eccentricities as high as $e = 1$ for the binary system. This allows for highly efficient GW emission from the system and decreases the merger timescale of the the system [6, 17, 19, 20, 21]. This increases the GW strain h and increases the detectability of the wave in the LISA detector band. While there exist previous papers which have modeled the GWs from such systems[6] and those which describe the effects of spinning SMBH on a binary[17] but no work has been done to combine the two together and modeled the GW strain of such a system.

5.1 Research Statement

We believe that there needs to be work done in modelling the effects of a spinning SMBH on the GW emission (especially their strain) from nearby binary as these signals may appear in the LISA band and the bands of any other future space based detectors. This work would allow for a ready matched filtering of such signal when LISA is in orbit and also in future works may allow to determine the rates at which these mergers occur in comparison to normal mergers.

5.2 Objectives

- To evaluate the detectability range for these events using present and future interferometer detectors.
- To generate templates for GWs from the inner binary of such a system, for matched filtering of the received signal

5.3 Methodology

The methodology for this research involves multiple steps to analyze the behaviour of GW from the hierarchical three-body system, particularly focusing on the inner orbit's dynamics under post-Newtonian corrections. First, we determine the parameter space for the model to ensure all relevant physical conditions and constraints are included.
Further, we model the gravitational wave (GW) strain, accounting for the evolving eccentricities in the inner and outer orbits under the LT influence. This includes generating synthetic GW noise corresponding to targeted detectors, such as LIGO and LISA [22], and plotting the power spectral density (PSD) for both the noise and the signal. By comparing these PSDs, we identify the points at which the signals would be detectable in each observatory. This comprehensive approach provides a rigorous examination of the impact of the KL mechanism on GW signals and merger dynamics, and allows us to bulid a framwork for modelling these systems in our future work, with potential implications for future astrophysical observations.

6 Results

6.1 Parameter Determination

Constraints

Stability of Hierarchical System

For KL oscillations to occur, the stability of the three body system must be maintained. For this reason, a necessary criteria is mentioned in [23], which predicts a minimum separation between the inner and outer orbits for stability, beyond which the system might become chaotic. This condition is given by

$$\frac{a_{out}}{a_{in}} > \frac{2.8}{1-e_{out}} \left[\frac{m_{out}}{m_{in}} \frac{1+e_{out}}{(1-e_{out})^{\frac{1}{2}}} \right]^{\frac{2}{5}} \tag{6.1.1}$$

However, as our outer orbit is considered to be circular, $e_{out} << 1$, giving us the scaled expression [6],

$$\frac{a_{out}}{AU} > 2.8 \left(\frac{m_{out}}{M_\odot} \right)^{\frac{2}{5}} \left(\frac{m_{in}}{M_\odot} \right)^{-\frac{2}{5}} \frac{a_{in}}{AU} \tag{6.1.2}$$

This gives us a lower bound for the separation between the two orbits.

Relativistic precession of periastron

KL oscillations are suppressed or maximum eccentricity is restricted by the periastron precession of inner binary. To constrain this effect, we consider the GR precession timescale

of periastron [6, 24] of the inner binary and compare it with the KL timescale (see (3.6)) to get the constraint whose scaled expression is of the form

$$\left(\frac{a_{\rm out}}{\rm AU}\right)^3 < 10^8(1-e_{\rm in}^2)^{\frac{3}{2}}\left(\frac{m_{\rm in}}{M_\odot}\right)^{-2}\left(\frac{a_{\rm in}}{\rm AU}\right)^4\left(\frac{m_3}{M_\odot}\right) \tag{6.1.3}$$

assuming $e_{out} << 1$.

Lense-Thirring Precession effect

For the Lense - Thirring effect to appear, we need to have a constraint such that $t_{KL} \geq t_{L_{out}S_3}$ (see (4.3)), for which the scaled expression [6] is given as

$$\left(\frac{a_{\rm in}}{\rm AU}\right)^{\frac{3}{2}} \leq 10^{-12}\left(\frac{m_3}{M_\odot}\right)\left(\frac{m_{\rm in}}{M_\odot}\right)^{\frac{1}{2}} \tag{6.1.4}$$

assuming $\chi_3 \sim 1$

Parameter Space and Final Models

Depending on the five models shown in the Table 1, we plot the constraints on a a_{in} and a_{out} plot to find the region of stability and find the a_{in} and a_{out} of each model as shown in Figure 1. Based on these initial models, we find the all the initial parameters for these models, as seen in Table 2.

Table 1: *Models*

Binary	$m_1[M_\odot]$	$m_2[M_\odot]$	$m_3[M_\odot]$	Model
SBH-SBH	10	10	10^9	A
SBH-SBH	20	50	10^9	B
SBH-SBH	50	50	10^{10}	C
IMBH-IMBH	10^3	10^5	10^{10}	D
SMBH-SMBH	10^6	10^6	10^{10}	E

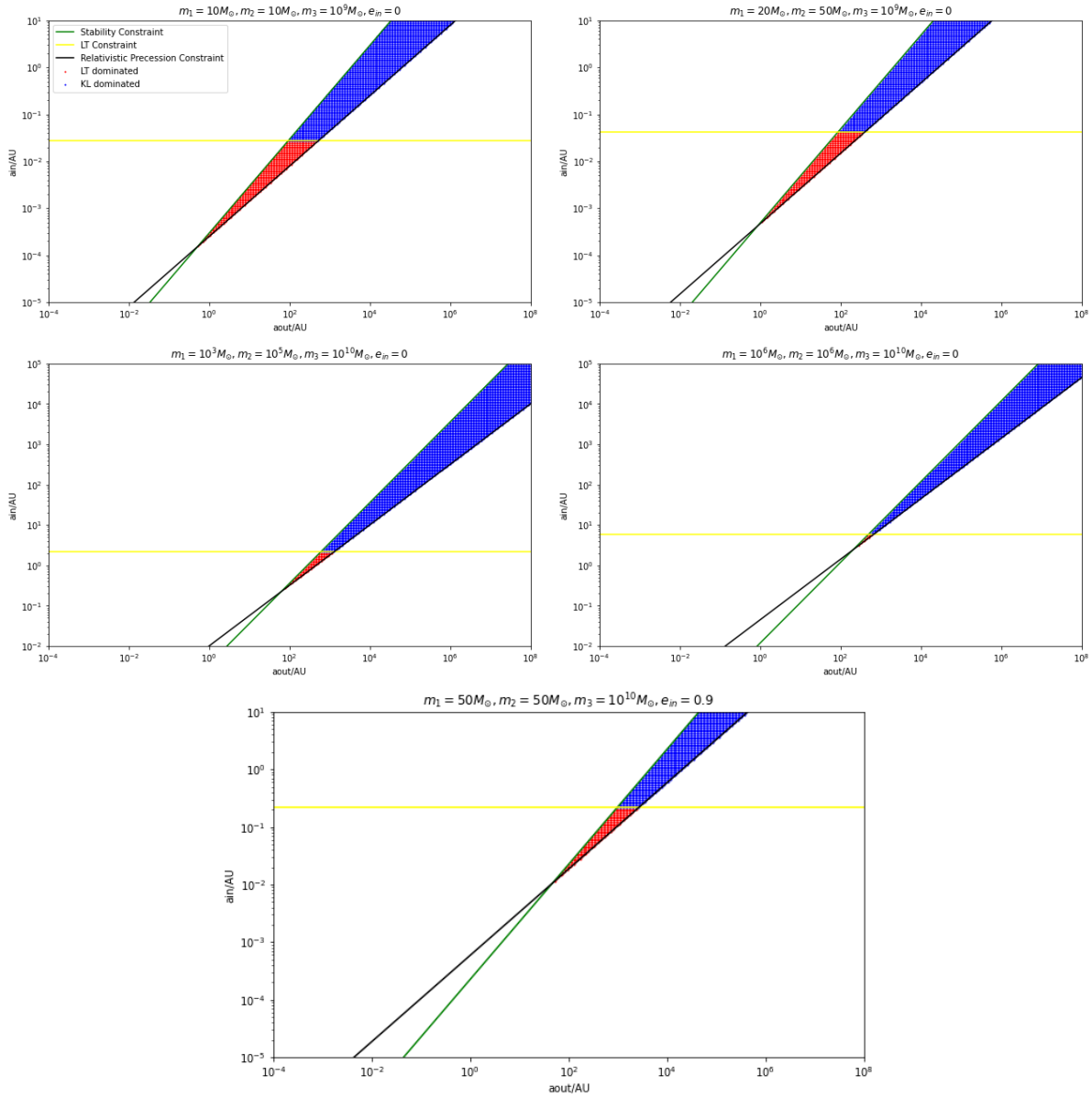

Figure 1: *The region between SC and RPC represents the allowed parameter space for stable KL oscillations. The red region shows (a_{in}, a_{out}) values for GW bursts dominated by Lense-Thirring (LT) precession, while the blue region indicates parameter space where bursts are KL-dominated. These phenomena occur only for $m_3 \geq 10^9\, M_\odot$.*

Table 2: *Model Parameters ($e_{out} \sim 0$)*

Model	$m_1[M_\odot]$	$m_2[M_\odot]$	$m_3[M_\odot]$	e_{in}	$a_{in}[AU]$	$a_{out}[AU]$	I [Deg]	$P_{in}[hrs]$	$P_{out}[days]$	$t_{KL}[yrs]$
A	10	10	10^9	0	0.027	301.3	90	8.67	60.42	27.60
B	20	50	10^9	0	0.041	236.5	90	8.67	42.02	13.34
C	50	50	10^{10}	0.9	0.215	1784.6	0	8.674	275.42	57.06
D	10^3	10^5	10^{10}	0	2.162	945.77	90	8.76	106.26	8.46
E	10^6	10^6	10^{10}	0	5.848	578.9	90	8.76	50.88	1.94

6.2 GWs from highly eccentric orbits

Gravitational waveform from a binary system strongly depends on the eccentricity of the orbit. In an eccentric orbit, the emission of gravitational waves is highly efficient and is distributed over many harmonics. The total radiation power P averaged over one period is given by

$$\mathcal{P} = \frac{32G^4 m_1^2 m_2^2 m_{\rm in}}{c^5 a_{\rm in}^5 (1-e_{\rm in}^2)^{7/2}} \left(1 + \frac{73}{24} e_{\rm in}^2 + \frac{37}{96} e_{\rm in}^4\right) \tag{6.2.1}$$

where a_{in} and e_{in} are the semi-major axis and the eccentricity of the inner binary, respectively. It shows that the radiation power increases rapidly as the eccentricity increases. The total radiation power P is the sum of the power radiated in the nth harmonic $\mathcal{P}_n$, given as

$$\mathcal{P} = \sum_{n=1}^{\infty} \mathcal{P}_n \tag{6.2.2}$$

where the power due to the nth harmonic is given by,

$$\mathcal{P}_n = \frac{32G^4 m_1^2 m_2^2 m_{\rm in}}{c^5 a_{\rm in}^5} g(n, e_{\rm in}) \tag{6.2.3}$$

where

$$\begin{aligned} g(n,e) = \frac{n^4}{32}\Bigg[&\Big(J_{n-2}(ne) - 2eJ_{n-1}(ne) + \frac{2}{n}J_n(ne) + 2eJ_{n+1}(ne) - J_{n+2}(ne)\Big)^2 \\ &+ (1-e^2)\Big(J_{n-2}(ne) - 2J_n(ne) + J_{n+2}(ne)\Big)^2 + \frac{4}{3n^2}\Big(J_n(ne)\Big)^2\Bigg] \end{aligned} \tag{6.2.4}$$

Here, $J_n(x)$ is the Bessel function of the first kind. The peak of the spectrum P_n is given by

$$f_{peak} = n_{peak} f_{in} \tag{6.2.5}$$

where f_{in} is the orbital frequency of the inner binary and n_{peak} is the magnification factor, which represents the number of harmonics. This factor can be approximated, in the range $10^{-6} < 1 - e^2 < 1$, to

$$n_{peak} = \frac{2(1+e)^{1.1954}}{(1-e^2)^{1.5}} \tag{6.2.6}$$

We can see that if eccentricity $e << 1$, $n_{peak} \sim 2$, describing the peak frequency of GWs from a circular orbit, whereas for high eccentricities, n_{peak} is very high and would be in the detectable range of the detector (10^{-4}Hz to 10kHz). Also, since the signal from a highly eccentric orbit consists many harmonics, the signal has a broad spectrum of frequencies.

We also check the strain of the wave at the nth harmonic, given by

$$\langle h_n^2 \rangle = (2\pi f_n)^2 \langle h_n^2 \rangle \approx \frac{4G}{c^3 D^2} P_n(a, e) \tag{6.2.7}$$

where f_n is the frequency of nth harmonic, D is the distance of the source. At $f_n = f_{peak}$, we can approximate the equation and express in scaled form as

$$\sqrt{\langle h_n^2 \rangle} \approx 5 \times 10^{-25}\, g^{1/2} \frac{(n_{\rm peak}, e)}{n_{\rm peak}} \left(\frac{m_1}{M_\odot}\right) \left(\frac{m_2}{M_\odot}\right) \times \left(\frac{a_{\rm in}}{\rm AU}\right)^{-1} \left(\frac{D}{10\ {\rm kpc}}\right)^{-1} \tag{6.2.8}$$

For $m_1 = m_2 = 10M\odot, a_{in} = 0.01AU, D = 10kpc$,

$$\sqrt{\langle h_n^2 \rangle} \approx 1.9 \times 10^{-22} \tag{6.2.9}$$

which is highly detectable in our present and future detectors.

6.3 Detector Noise Curves

The noise curves of detectors play a crucial role in determining the detectability of various sources. These curves illustrate the sensitivity of the detector across different frequency ranges, providing valuable insights into its performance. To obtain these noise curves, we analyze noise measurements collected by sensors in the time domain. By performing a Fast Fourier Transform (FFT) on this data, we can calculate the Power Spectral Density (PSD) of the noise. Alternatively, an analytical equation for the noise specific to the detector can also be employed. For our purposes, the analytical noise $S_n(f)$ proves to be sufficient, allowing us to effectively assess the detector's capabilities.

aLIGO

The Advanced Laser Interferometer Gravitational-Wave Observatory (aLI-GO) [25] is a highly sensitive instrument designed to detect gravitational waves, or ripples in spacetime, resulting from cosmic events such as black hole and neutron star mergers. Operational since its major upgrade in 2015, aLIGO consists of twin facilities located in Livingston,

Louisiana, and Hanford, Washington, each equipped with interferometers that utilize laser beams and mirrors across four-kilometer arms to detect minuscule distortions caused by passing gravitational waves. aLIGO has achieved breakthroughs in astrophysics, including the first confirmed gravitational wave detection from a binary black hole merger.. Through continual upgrades, including advanced quantum noise reduction techniques, aLIGO's sensitivity has increased, enabling it to observe a larger volume of the universe, capture faint signals, and detect more frequent events, furthering our understanding of the universe's fundamental properties. aLIGO's noise curve equation [26] is given by

$$S_n(f) = \begin{cases} S_0 \left[x^{-4.14} - 5x^{-2} + 111 \left(\frac{1 - x^2 + \frac{x^4}{2}}{1 + \frac{x^2}{2}} \right) \right], & \text{for } f \geq f_s \\ \infty, & \text{for } 0 < f < f_s \end{cases} \tag{6.3.1}$$

where $f_s = 10\,\text{Hz}$ is the cutoff frequency of detector, $f_0 = 215\,\text{Hz}$ is the characteristic frequency of the detector, $x = \frac{f}{f_0}$, $S_0 = 10^{-49}\,\text{Hz}^{-1}$ is the reference noise level. This gives us the sensitivity curve of the detector, which shows us the detectability of any signal as shown in Figure 2.

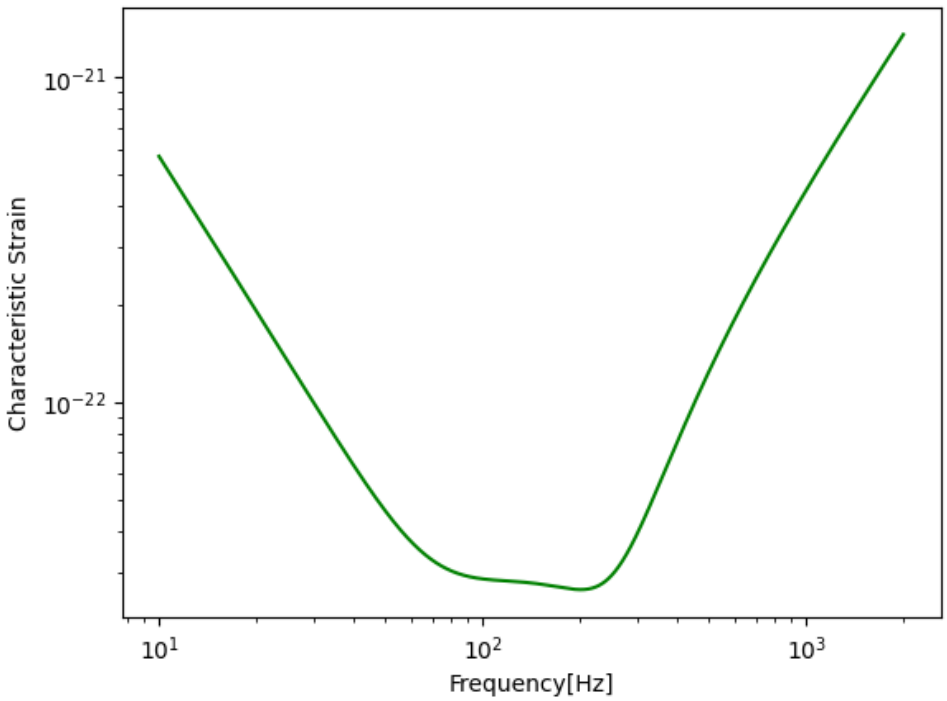

Figure 2: *Sensitivity curve of the Advanced LIGO (aLIGO) detector.*

LISA

The Laser Interferometer Space Antenna (LISA) [25] is an ambitious gravitational wave observatory set to be launched by the European Space Agency (ESA), with participation from NASA, targeting an operational period in the 2030s. Unlike ground-based detectors like LIGO and Virgo, LISA will operate in space, allowing it to detect gravitational waves at much lower frequencies. It comprises three spacecraft arranged in an equilateral triangle with 2.5 million kilometers between each pair [22]. LISA is designed to capture gravitational waves produced by massive celestial events, such as mergers of supermassive black holes, inspirals of stellar-mass compact objects into supermassive black holes, and potentially signals from the early universe.

LISA's low-frequency sensitivity opens a window to events beyond the reach of current ground-based interferometers. These events can reveal crucial insights into galaxy formation, cosmology, and fundamental physics. Orbiting the Sun in tandem with Earth, LISA's constellation will effectively remove terrestrial noise sources, providing a pristine environment for gravitational wave detection. The data from LISA will complement observations from high-frequency detectors on Earth, expanding our understanding of the universe through multi-frequency gravitational wave astronomy. The sensitivity curve for LISA [22] is given by

$$S_n(f) = \frac{P_n(f)}{\mathcal{R}(f)} \tag{6.3.2}$$

where $P_n(f)$ is the power spectral density of the noise, and $\mathcal{R}(f)$ is the response function of the detector.

Here, $P_n(f)$ is given by,

$$P_n(f) = \frac{P_{\text{OMS}}}{L^2} + 2\left(1 + \cos^2\left(\frac{f}{f_*}\right)\right)\frac{P_{\text{acc}}}{(2\pi f)^4 L^2} \tag{6.3.3}$$

where P_{OMS} is the single optical metrological noise, and P_{acc} is the single test mass acceleration noise.

And, the response function $\mathcal{R}(f)$ is given by,

$$\mathcal{R}(f) = \frac{3}{10}\frac{1}{\left(1 + 0.6\left(\frac{f}{f_*}\right)^2\right)} \tag{6.3.4}$$

Thus, the sensitivity curve $S_n(f)$ is

$$S_n(f) = \frac{10}{3L^2}\left(P_{\text{OMS}} + 2\left(1 + \cos^2\left(\frac{f}{f_*}\right)\right)\frac{P_{\text{acc}}}{(2\pi f)^4}\right)\left(1 + \frac{6}{10}\left(\frac{f}{f_*}\right)^2\right) \tag{6.3.5}$$

where $L = 2.5\,\mathrm{Gm}$ and $f_* = 19.09\,\mathrm{mHz}$.

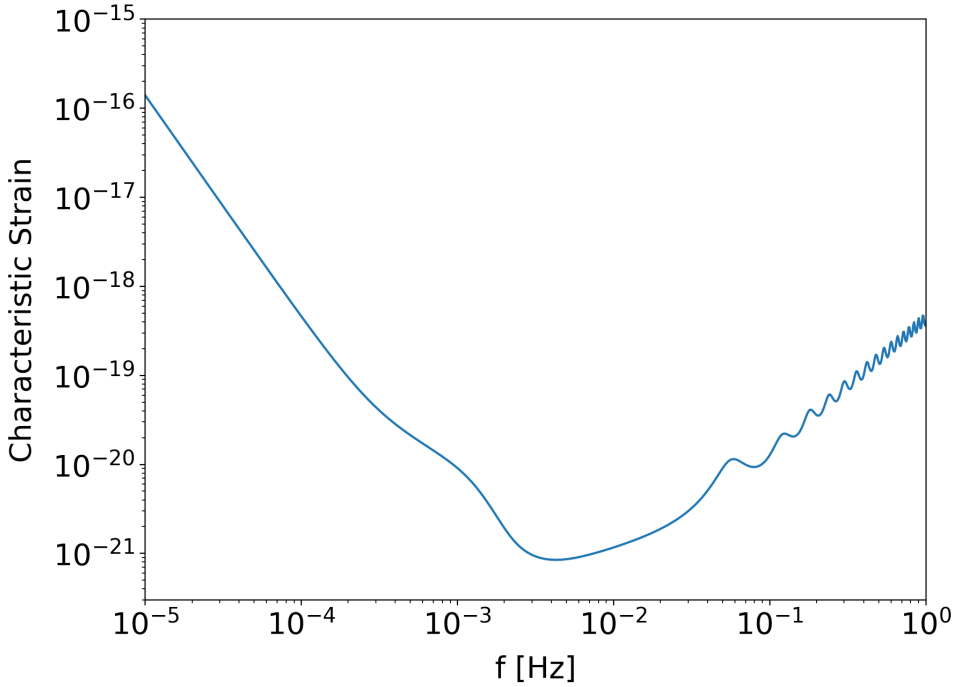

Figure 3: *Sensitivity curve of the LISA detector.*

6.4 Frequency Ringdown

Now, that we have our sensitivity curves for both detectors, we can see the whether our models are detectable by the detectors. We have considered the mergers when our models reach an eccentricity of 0.9, using the EccentricFD approximant in the PyCBC [27] python package. From our results, we can divide up the models into two sets, one set consisting of SBH binaries at the Galactic Centre of our galaxy and the other consisting of IMBH and SMBH binaries at a distance of 100Mpc. Figure 4 shows the first set and Figure 5 represents the second set of mergers.

These, results show that binaries in eccentric orbits are mostly visible in the LISA frequency range and that the peaks in the plot of the GWs from these mergers represent the final stage before entering merger phase, if the orbits never lose their eccentricity. However, these orbits tend to circularize after reaching such eccentricities creating an evolving system. From our numerical calculation we have found that, below 10Mpc, SMBH binaries at high eccentricities are not visible in LISA frequency range.

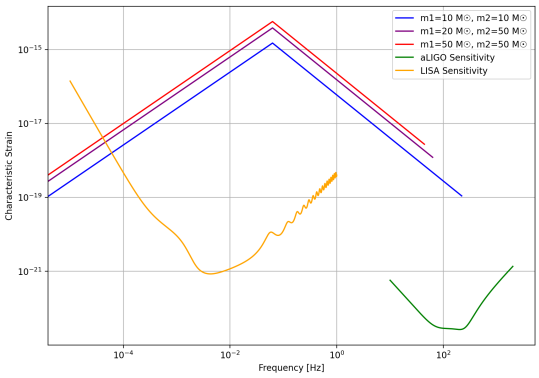

Figure 4: *SBH binaries at Galactic Centre*

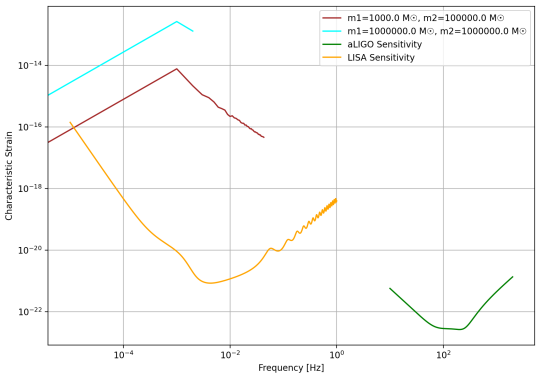

Figure 5: *IMBH and SMBH binaries at 100Mpc*

However, do note that these are rough simulations based on already existing approximants in the PyCBC pipeline and the final results from the orbit evolved GWs may vary slightly from these results.

7 Future Work

7.1 Orbit Evolution

We shall use the below 1PN Einstein-Hoffman-Infeld n-body equations of motion [28] to find the osculating elements of the orbit.

$$\begin{aligned}\frac{d\vec{v}_k}{dt} =& -G\sum_{n\neq k} m_n \frac{\vec{x}_k-\vec{x}_n}{|\vec{x}_k-\vec{x}_n|^3}\left[1-\frac{4G}{c^2}\sum_{n'\neq k}\frac{m_{n'}}{|\vec{x}_k-\vec{x}_{n'}|}-\frac{G}{c^2}\sum_{n'\neq n}\frac{m_{n'}}{|\vec{x}_n-\vec{x}_{n'}|}\left(1-\frac{(\vec{x}_k-\vec{x}_n)\cdot(\vec{x}_n-\vec{x}_{n'})}{2|\vec{x}_n-\vec{x}_{n'}|^2}\right)\right]\\ &+\left(\frac{|\vec{v}_k|}{c}\right)^2+\left(\frac{|\vec{v}_n|}{c}\right)^2+2\frac{\vec{v}_k\cdot\vec{v}_n}{c^2}-\frac{3}{2}\left(\frac{(\vec{x}_k-\vec{x}_n)\cdot\vec{v}_n}{|\vec{x}_k-\vec{x}_n|}\frac{\vec{v}_n}{c}\right)^2\\ &-\frac{7G^2}{2c^2}\sum_{n\neq k}\frac{m_n}{|\vec{x}_k-\vec{x}_n|}\sum_{n'\neq n}\frac{m_{n'}(\vec{x}_n-\vec{x}_{n'})}{|\vec{x}_n-\vec{x}_{n'}|^3}-\frac{G}{c^2}\sum_{n\neq k} m_n\frac{\vec{v}_k-\vec{v}_n}{|\vec{x}_k-\vec{x}_n|^3}(\vec{x}_k-\vec{x}_n)\cdot(3\vec{v}_n-4\vec{v}_k)\end{aligned}$$

where $m_k, v_k, x_k (k = 1, 2, 3)$ are the mass, velocity and position of the kth component of the system. The above equation is numerically integrated using the 6th-order implicit Runge-Kutta method [29, 30] in order to find the positions and velocities of the masses and find the osculating elements.

We will do the same for a 1.5PN n-body eqautions of motion in order to find osculating elements when the Lense-Thirring effect is including.

7.2 GW Modelling

We will use the evolving positions obtained from the 1PN orbit evolution and put them through the GW radiation equations for an eccentric orbit [31, 32]. Another method,

given by is using the mass quadrupole moment for N masses

$$M_{ij} = \sum_{\Lambda=1}^{N} m_A x_A^i x_A^j \tag{7.2.1}$$

where we can substitute the positions obtained from the the orbit evolution. This is substituted in the reduced quadrupole moment

$$Q_{ij} = M_{ij} - \frac{1}{3}\delta_{ij} M_k^k \tag{7.2.2}$$

and then can be substituted in the tranverse-traceless gauge metric:

$$h_{ij}^{TT}(t,x) = \frac{2G}{Dc^4}\ddot{Q}_{ij}^{TT} \tag{7.2.3}$$

The waveform extracted are expected to be in the time domain (TD). This data is to be put through LISA's GW response code [33], providing us data points that will allow us to find the evolution of strain over time for such systems. Then we shall apply a Fourier transform over the TD data and get it in frequency domain (FD). This will allow us to see how the waveform is actually observable in the chosen detectors.

Bibliography

[1] S. Ray, R. Bhattacharya, S. Sahay, A. Aziz, and A. Das, "Gravitational wave: Generation and detection techniques," *International Journal of Modern Physics D*, 12 2023.

[2] B. Abbott, R. Abbott, T. Abbott, M. Abernathy, F. Acernese, K. Ackley, C. Adams, T. Adams, P. Addesso, R. Adhikari, V. Adya, C. Affeldt, M. Agathos, K. Agatsuma, N. Aggarwal, O. Aguiar, L. Aiello, A. Ain, P. Ajith, and B. Allen, "Observation of gravitational waves from a binary black hole merger," *Physical Review Letters*, vol. 116, Feb. 2016.

[3] Rich Abbott, Thomas D. Abbott, Sheelu Abraham, Fausto Acernese, Kendall Ackley, Carl Adams, Rana X. Adhikari, Vaishali B. Adya, Christoph Affeldt, Michalis Agathos, Kazuhiro Agatsuma, Nancy Aggarwal, Odylio D. Aguiar, Amit Aich, Lorenzo Aiello, Anirban Ain, Ajith Parameswaran, and Gabrielle Allen, "Open data from the first and second observing runs of advanced ligo and advanced virgo," *SoftwareX*, vol. 13, p. 100658, Jan. 2021.

[4] Y. Aso, Y. Michimura, K. Somiya, M. Ando, O. Miyakawa, T. Sekiguchi, D. Tatsumi, and H. Yamamoto, "Interferometer design of the kagra gravitational wave detector," *Physical Review D*, vol. 88, Aug. 2013.

[5] P. Amaro-Seoane, H. Audley, S. Babak, J. Baker, E. Barausse, P. Bender, E. Berti, P. Binetruy, M. Born, D. Bortoluzzi, J. Camp, C. Caprini, V. Cardoso, M. Colpi, J. Conklin, N. Cornish, and C. Cutler, "Laser interferometer space antenna," 2017.

[6] P. Gupta, H. Suzuki, H. Okawa, and K.-i. Maeda, "Gravitational waves from hierarchical triple systems with kozai-lidov oscillation," *Phys. Rev. D*, vol. 101, p. 104053, May 2020.

[7] J.Narlicker, *An Introduction to Relativity*. The Edinburgh Building, Cambridge CB2 8RU, UK: Cambridge University Press, 1 ed., 2010.

[8] S. Bose, *An Introduction to General Relativity*. 4835/24 Ansari Road, Daryaganj, New Delhi 110002, India: Wiley Eastern Limited, 1 ed., 1980.

[9] D. Blair, L. Ju, C. Zhao, *et al.*, "Gravitational wave astronomy: the current status," *Science China Physics, Mechanics & Astronomy*, vol. 58, p. 120402, 2015.

[10] Y. Kozai, "Secular perturbations of asteroids with high inclination and eccentricity," *Astrophysical Journal*, vol. 67, pp. 591–598, Nov. 1962.

[11] M. Lidov, "The evolution of orbits of artificial satellites of planets under the action of gravitational perturbations of external bodies," *Planetary and Space Science*, vol. 9, no. 10, pp. 719–759, 1962.

[12] S. Naoz, "The eccentric kozai-lidov effect and its applications," *Annual Review of Astronomy and Astrophysics*, vol. 54, p. 441–489, Sept. 2016.

[13] C. D. Murray and S. F. Dermott, *Solar System Dynamics*. Cambridge University Press, 2000.

[14] I. Shevchenko, *The Lidov-Kozai Effect - Applications in Exoplanet Research and Dynamical Astronomy*, vol. 441. Springer Cham, 01 2017.

[15] J. M. O. Antognini, "Timescales of kozai-lidov oscillations at quadrupole and octupole order in the test particle limit," *MNRAS*, vol. 452, pp. 3610–3619, Oct. 2015.

[16] H. Pfister, "On the history of the so-called Lense-Thirring effect," *General Relativity and Gravitation*, vol. 39, pp. 1735–1748, Nov. 2007.

[17] Y. Fang, X. Chen, and Q.-G. Huang, "Impact of a spinning supermassive black hole on the orbit and gravitational waves of a nearby compact binary," *The Astrophysical Journal*, vol. 887, p. 210, Dec. 2019.

[18] Y. Fang and Q.-G. Huang, "Secular evolution of compact binaries revolving around a spinning massive black hole," *Phys. Rev. D*, vol. 99, p. 103005, May 2019.

[19] B. Liu, D. Lai, and Y.-H. Wang, "Binary mergers near a supermassive black hole: Relativistic effects in triples," *The Astrophysical Journal Letters*, vol. 883, p. L7, Sept. 2019.

[20] J. H. VanLandingham, M. C. Miller, D. P. Hamilton, and D. C. Richardson, "The role of the kozai–lidov mechanism in black hole binary mergers in galactic centers," *The Astrophysical Journal*, vol. 828, p. 77, Sept. 2016.

[21] Z. Xuan, S. Naoz, B. Kocsis, and E. Michaely, "Detecting gravitational wave bursts from stellar-mass binaries in the mhz band," *The Astrophysical Journal*, vol. 965, p. 148, 04 2024.

[22] T. Robson, N. J. Cornish, and C. Liu, "The construction and use of lisa sensitivity curves," *Classical and Quantum Gravity*, vol. 36, p. 105011, Apr. 2019.

[23] R. A. Mardling and S. J. Aarseth, "Tidal interactions in star cluster simulations," *MNRAS*, vol. 321, pp. 398–420, Mar. 2001.

[24] O. Blaes, M. H. Lee, and A. Socrates, "The kozai mechanism and the evolution of binary supermassive black holes," *The Astrophysical Journal*, vol. 578, p. 775–786, Oct. 2002.

[25] B. P. Abbott, R. Abbott, R. Adhikari, P. Ajith, B. Allen, G. Allen, *et al.*, "LIGO: the Laser Interferometer Gravitational-Wave Observatory," *Reports on Progress in Physics*, vol. 72, p. 076901, July 2009.

[26] "Summer school on gravitational-wave astronomy," International Centre for Theoretical Sciences, 2024.

[27] T. P. Team, "Pycbc: Gravitational wave data analysis." `https://github.com/gwastro/pycbc`, 2024. Accessed: 2024-10-31.

[28] A. Einstein, L. Infeld, and B. Hoffmann, "The gravitational equations and the problem of motion," *Annals of Mathematics*, vol. 39, no. 1, pp. 65–100, 1938.

[29] H. A. Luther, "An explicit sixth-order runge-kutta formula," *Mathematics of Computation*, vol. 22, no. 102, pp. 434–436, 1968.

[30] J. C. Butcher, "Implicit runge-kutta processes," *Mathematics of Computation*, vol. 18, pp. 50–64, 1964.

[31] R. S. Chandramouli and N. Yunes, "Ready-to-use analytic model for gravitational waves from a hierarchical triple with kozai-lidov oscillations," *Physical Review D*, vol. 105, Mar. 2022.

[32] P. C. Peters and J. Mathews, "Gravitational radiation from point masses in a keplerian orbit," *Phys. Rev.*, vol. 131, pp. 435–440, Jul 1963.

[33] J.-B. Bayle, Q. Baghi, A. Renzini, and M. Le Jeune, "LISA GW Response," Feb 2023. Zenodo.